



RESEARCH MEMORANDUM

PERFORMANCE OF A TWO-DIMENSIONAL CASCADE INLET AT A
FREE-STREAM MACH NUMBER OF 3.05 AND AT ANGLES OF
ATTACK OF -3° , 0° , 3° , AND 6°

By Richard R. Woollett and Harold M. Ferguson

Lewis Flight Propulsion Laboratory
Cleveland, Ohio

NATIONAL ADVISORY COMMITTEE
FOR AERONAUTICS
WASHINGTON

March 5, 1958
Declassified December 8, 1961

NACA RM E57L06

NATIONAL ADVISORY COMMITTEE FOR AERONAUTICS

RESEARCH MEMORANDUM

PERFORMANCE OF A TWO-DIMENSIONAL CASCADE INLET AT A FREE-STREAM
MACH NUMBER OF 3.05 AND AT ANGLES OF ATTACK OF -3° , 0° , 3° , AND 6°

By Richard R. Woollett and Harold M. Ferguson

SUMMARY

A double-ramp cascade inlet was investigated at a Mach number of 3.05 in order to ascertain the penalties associated with decreasing the length of inlets by means of cascades. Total-pressure recovery and profile distortion of the cascade inlet were compared with a similar single-passage inlet that captured the same mass flow. The critical total-pressure recoveries of the cascade and single-passage inlet were 0.56 and 0.59, respectively, although the peak recoveries were 0.56 and 0.62, respectively. This 0.03 to 0.06 loss in recovery was accompanied by an improvement in profile distortion. However, a rather severe pressure and mass-flow discontinuity exists when the cascade inlet goes into subcritical operation. Pressure recovery decreased from the previously mentioned value to 0.38, while the mass flow dropped from 1 to 0.64. In addition, positive angle-of-attack performance was extremely penalized; the total-pressure recovery dropped approximately 0.28 percentage points for a positive angle of attack of 6° .

The effect of maintainance of separate flow passages throughout the inlet had no discernible effect upon the critical and supercritical inlet performance.

INTRODUCTION

The ducting between the entrance of a supersonic inlet and the compressor face can assume an undesirable length in present-day and future high-speed aircraft, primarily because of the slow diffusion rates required for high-performance subsonic diffusers. The length can be decreased by increasing the rate of subsonic diffusion and accepting the resulting total-pressure losses. Another method that can be used to

shorten the inlet is the cascade principle. If a group of small inlets are arranged in such a manner that the "starting" condition of any one is not altered by the grouping, a considerable reduction in diffuser length can be realized. In addition to a reduction in diffuser length, there are several other advantages associated with the cascade design.

Any phenomenon which is a function of diffuser length will be affected by the use of a cascade inlet. If the profiles associated with a particular inlet are poor, ample mixing length must be provided in order to obtain uniform profiles. However, nonuniform flows discharging from the exits of a group of small diffusers into a common chamber tend to mix more rapidly than flows discharging from a single large diffuser. Consequently, mixing length should be substantially shorter with cascade diffusers.

Not only will length dimensions be substantially reduced by cascading the inlet, but the height measurements of individual elements will be reduced. The projected cowl area and, consequently, cowl pressure drag would thus be reduced, since only one element contributes to the external drag. The frontal area of the other elements are used in the compressions of the internal flow. Of course, any projected area present on side plates would not diminish.

So far the discussion applies equally well to axially symmetric inlets, side inlets, and two-dimensional inlets. Each type, though, has particular advantages and drawbacks. In addition to the advantage of flat surfaces that may be so controlled that off-design flight operation is possible, a certain degree of versatility in application exists with two-dimensional cascade-type inlets. The total captured mass flow and, consequently, thrust could be varied by stacking a number of individual elements for use in a variety of missiles.

Much work has been done with two-dimensional single-passage diffusers at various Mach numbers but little data exist for the cascade inlet. Data presented at Mach 3 (ref. 1) indicate that a pressure recovery of 0.45 is possible for a cascade diffuser. However, no evaluation of the cascade relative to a single-passage inlet was made. The recovery that was obtained in reference 1 could probably be increased by designing for a higher theoretical performance. An experimental investigation of a high performance (theoretical) cascade inlet at a Mach number of 3 was undertaken in order to ascertain the relative merits of this type of inlet. The elements of the cascade were designed in the same manner as a single-passage configuration previously tested at the Lewis laboratory (ref. 2).

4406
SYMBOLS

m mass-flow rate

P total pressure

p static pressure

α angle of attack

Δ increment

Subscripts:

av average

0 free-stream values

APPARATUS AND PROCEDURE

Tests were conducted in the 18- by 18-inch supersonic wind tunnel at a free-stream Mach number of 3.05 and simulated pressure altitude of 80,000 feet. Reynolds number based on body height (4 in.) was 0.5×10^6 and dewpoint temperatures ranged from -25° to -5° F.

The individual elements of this inlet were the same as the double-wedge inlet of reference 2. The leading edges of the three elements are staggered to form an angle equal to the oblique shock angle of the initial 10° deflection of the first wedge. The second wedge of the double-wedge compression surface deflected the flow an additional 15° with its oblique shock theoretically intersecting the initial shock at the leading edge of the lip. A near-maximum internal contraction (for self starting) was incorporated in the design. This necessitated turning the flow at the lip 7° back towards axial.

Because these elements are so canted, the length of the cascade L_c is given by

$$L_c = \frac{L}{n} + \frac{D}{\tan \phi} \frac{n-1}{n}$$

where L is the length of the equivalent single-passage comparison inlet, D its height, ϕ the sweep angle, and n is the number of passages in the cascade configuration. For the three-passage inlets investigated, the reduction in length was approximately one-half. However, the total wetted surface of the diffuser was about eight-tenths that of a single-passage inlet, indicating, perhaps, that a reduction in weight as well as size can be realized.

The cowl pressure drag associated with the cascade configuration will be approximately $1/n$ times the pressure drag of the comparison inlet. This drag reduction may not be realized, however, since cascading a two-dimensional inlet will not decrease the pressure drags of the side plates. If the side-plate drag is assumed to be one-half the total and is not reduced by cascading, the pressure drag associated with the cascade configuration will be approximately $(n+1)/2n$ times that of the comparison inlet.

In the present investigation, three diffusion passages were selected mainly because of existing parts and tunnel size. No optimization was considered. The present configuration decreased diffusion length by roughly 50 percent and cowl projected area by 44 percent.

An inside view of the three-element, single settling-chamber model including the chamber pressure instrumentation is shown in figure 1(a). Mass flow is controlled by a single plug at the settling-chamber exit. Mass-flow ratios were obtained from measurements of the static- and total-pressure ratios for known values of exit- to settling-chamber area ratios. A variation of internal contraction was affected by translatory movement of the elements in a streamwise direction.

Instrumentation consisted of static-pressure orifices in the throat and the subsonic diffuser, a downstream rake station, and a total-pressure probe that translated in the plane formed by the trailing edges of the elements. Two Statham gages connected to orifices on the top and the side of the settling chamber were used for measuring pressure fluctuations. A schematic diagram of the model and the instrumentation is shown in figures 2(a) and (b).

Figure 1(b) shows a variation of this model with the two bottom passages inoperative and with the changes in instrumentation for this test, including a new total-pressure rake at the diffuser exit. However, the static-pressure orifices for this passage, the downstream total-pressure rake, and the exit plug are the same as for the model shown in figure 1(a).

An additional three-passage (cascade) inlet was investigated, in which the passages were separated to the exit, forming essentially three individual inlets. Mass flow in each passage was controlled by an individual exit butterfly valve. Locations of static-pressure orifices in the throat and of the diffuser total-pressure rake were the same as in the other inlets. Mass flow in each of the individual passages of the triple-exit cascade was determined from static pressures and area ratio across an exit nozzle.

RESULTS AND DISCUSSION

Zero-Angle-of-Attack Performance

Pressure recoveries and fluctuations. - The principal advantages of the two-dimensional cascade inlet are associated with its space-saving features and reduction in cowl drag. These advantages, however, must be compared with a probable decrease in inlet performance. The pressure performance of the cascade inlet that has a common plenum chamber and single exit is presented in figure 3 along with the performance of the previously tested double-wedge inlet. Representative schlieren photographs taken at various operating conditions are presented in figure 4. As the back pressure in the settling chamber was gradually increased, the total-pressure recovery increased at constant, near unity, mass flow to a value of 0.56. Beyond this point, the normal shock was expelled from the bottom passage and positioned itself ahead of the entrance. The inlet would then operate at a condition (branch B) where the pressure recovery was 0.375 and the mass flow, 0.64. Since the reduction in mass flow was larger than 1/3, flow reversal (a net upstream flow) existed in the bottom inlet, while the middle and the top passages were operating supercritically. Reduction of the back pressure gave noticeable evidence of a hysteresis loop where the shock again reswallowed (dashed lines, fig. 3(a)). The operating conditions (branch B) necessary for the bow shock to reswallow were rather uncertain since they varied from run to run and were probably responsible for the error in the slope of the discontinuity line. With the inlet operating on branch B, a change in the bow shock configuration (from weak to strong shock) occurred ahead of the bottom passage at a definite value of mass flow. This change in bow-shock configuration (see fig. 4) was accompanied by a shift in diffuser operation to branch C of the curve of the total-pressure ratio P/P_0 against mass-flow ratio m/m_0 . The shock pattern then remained

essentially unchanged for a range in reduced mass flow until a second so-called "critical point" was reached, at which time the normal shock was expelled from the middle passage.

The pressure fluctuations in the settling chamber that are presented in figure 3(b) varied considerably during subcritical operation. They became quite large at the lower mass flows and thus eliminated the hysteresis loop between branches C and D (fig. 3(a)). In addition, there were specific regions of mass-flow operation where pressure fluctuation $\Delta p/P$ (fig. 3(b)) became quite large. If the bottom passage operated subcritically (branch B, fig. 3(a)), a high fluctuation occurred when the mass flow was increased (fig. 3(b)). Operating conditions for extremely low values of mass flow were not obtained because of the magnitude of these disturbances. Although the magnitude of the pressure perturbations in the settling chamber was low in certain regions of mass flow, the size of the pressure change at the discontinuity was rather large.

The static-pressure distributions of the cascade diffusion process are presented for critical-point data in figure 5(a). Evidence that the flow near the throat was far from uniform and one-dimensional was obtained by noting that static pressures on adjacent walls of the same passage were not identical. For comparison, the wall static pressures for various operating conditions are presented in figures 5(b), (c), and (d). The extreme flatness of the static-pressure profiles in the subcritical passages indicates very low flow rates. Both forward and rearward facing total-pressure tubes placed in the diffuser indicated flow reversal during subcritical operation. In addition, it may be seen from figure 5(b) that since the terminal shock in the diffuser does not cause a distinct static-pressure rise, considerable boundary-layer separation must exist.

Flow distortion. - The effect of reverse flow and boundary-layer separation upon the total-pressure profile is seen in figure 6, where the profiles are plotted for various operating conditions. In addition to the profiles at the diffuser exit, profiles are also presented at a downstream station that is 10 inches upstream of the diffuser exit of the comparison single-passage inlet. The profile distortion at critical operation is 14.5 percent at the cascade diffuser exit and 3.6 percent at the downstream measuring station. For the single-passage comparison inlet, the distortion was 10 percent at a station farther downstream than the rearward measuring station of the cascade. Consequently, for equal lengths of diffusion plus mixing, the cascade inlet yielded lower distortions. As can be seen in figure 6(a), the pressure fluctuation was approximately the same for each of the three passages. Moreover, the flow between any two adjacent passages seems to be symmetric about the splitter plates; for example, if the flow separates on the lip side of the bottom passage, it separates off the wedge side of the middle passage and the lip side of the top passage. At subcritical operation, a similar

effect was noticed (fig. 6(b)) in that the low-pressure side of one supercritical passage was always adjacent to the low-pressure side of the other supercritical passage. The total-pressure profiles for a condition in which only one of the three inlets is operating supercritically is presented in figure 6(c). The distortion in the supercritical passage is quite high, being on the order of 63 percent. This is caused by the highly supercritical operation of that passage since the exit static pressure of the three passages should be identical. However, at the downstream measuring station the pressure fluctuation is low, being close to zero.

Comparison with single-passage inlet. - For comparison purposes, the performance of a single-passage inlet, which was designed in the same way as the cascade diffuser and which captured roughly the same mass flow, is presented in figure 3(a). The total-pressure recovery of the cascade inlet is 0.03 to 0.06 lower than the single-passage inlet depending upon whether the comparison is made between critical or maximum recovery points. It is somewhat difficult to determine whether this loss (comparing critical points) is due to the additional friction surfaces or due perhaps to a misalignment of the cascade passage. Since the individual inlets are rather small and internal contraction was incorporated in the design, there was some difficulty in matching the contraction of the three passages. Because of the nonuniformity of the flow in the throat section, it was impossible to ascertain symmetry of the three passages from static-pressure data.

The effect of longitudinal element misalignment (misaligned tip projection) in the cascade inlet was investigated by varying the internal contraction of the three passages. The tip projection of each element was so varied that the internal contraction ratio changed from 1.19 to 1.09. Performance of this inlet is presented in figures 7(a) and (b) and indicates only a slight change in total-pressure recovery (0.01) and a 0.04 to 0.05 change in mass-flow ratio. The recovery difference could be within the consistency of the data. A schlieren photograph at supercritical conditions is presented in figure 7(c).

The origin of some of the losses associated with the cascade can be determined by comparing the cascade performance with that of a single element. This comparison was accomplished by inserting a wooden block in the middle and bottom passages. The variation of total pressure with mass flow and the total-pressure profile obtained at the peak recovery point are presented in figures 8(a) and (b), respectively. The critical point is very close to that obtained for the larger single-passage comparison inlet. The peak total-pressure recovery, though, is not as large perhaps because of the absence of stable subcritical operation. This would indicate that there is no effect of scale or Reynolds number based on inlet height on the pressure recovery (in the range investigated) and that the difference in performance cannot be attributed to difference

in size. However, the off-design cascade inlet, purposely misaligned, indicated that small changes in internal contraction could not account for all the difference in the recovery. In addition, since the total surface area has not increased for the cascade, the losses probably cannot be assigned to an increased friction drag. Another possible contributing factor, other than misalignment and friction, may account for the unexplained portion of the total-pressure-recovery difference. The total-pressure profiles near critical (fig. 5) indicate that the flow did not always separate on the same side of the diffusion duct. Consequently, terminal-shock location and critical-point recovery may be different for the various passages.

Angle-of-Attack Performance

Pressure recoveries. - Because of the interdependence of operation of the three elements in the cascade diffuser, the angle-of-attack performance is of added interest. The performances at 3° , 6° , and -3° are presented in figure 9. The peak total-pressure recoveries at these three conditions are 0.38, 0.275, and 0.44, respectively, whereas the corresponding mass flows are 0.86, 0.65, and 0.91. At positive angle of attack, the inlet operated considerably different from zero angle, that is, there were no longer distinct branches and hysteresis loops on the total-pressure performance curves. This was undoubtedly due to the strong detached shocks always present during supercritical operation, which eliminate the internal compression of the inlet, permitting variation in mass flow without changes in the initial shock structure. Photographs of these shock structures are presented in figures 10(a) and (b); the negative angle of attack is presented in figure 10(c). The settling-chamber static-pressure fluctuations for these angles of attack are presented in figure 9.

Flow distortion. - The effect of angle of attack upon the total-pressure distortion is presented in figure 11 for critical-point operation. The percentage of distortion becomes quite large at positive angle of attack, reaching a value of 50 percent at 3° and 83 percent at 6° . Even the downstream station has a rather high distortion, about 20 percent at 6° angle of attack. At a 3° angle of attack, distortions are comparable with zero-angle-of-attack data. Average total pressures of each of the three passages are no longer identical as at zero angle of attack. At an angle of attack of 3° there is a difference of 0.10 between the peak total-pressure recovery of the top and bottom passages; at 6° there is a difference of 0.18; and at -3° the bottom passage has 0.06 higher recovery than the top passage. Unfortunately, there are no angle-of-attack data for the comparison model.

Effect of Maintaining Separate Flow Passages

The peak total-pressure recovery and supercritical mass flow for the configuration having three separated passages and exits are presented in figure 12 plotted against angle of attack. The peak performance of the various passages differs greatly at angle of attack. The performance of the cascade with common plenum and single exit is also included in the figure for comparison. It can be seen that the top passage has the best over-all recovery up to an angle of attack of 6° , changing very little. However, the bottom passage has a higher recovery than the middle passage, a result that would not be expected. A possible explanation is that the bow shock standing in front of the middle passage has weakened sufficiently when it passes through the bottom-passage stream tubes to improve the over-all total-pressure recovery. The performance of the single-exit cascade diffuser is also shown for comparison. The same trends, and consequently the same conclusion, were obtained for the mass-flow relation.

Total-pressure profiles are presented in figure 13 for various angles of attack at the critical operative condition. It can be seen that the high total-pressure recovery region is always on the wedge side of the passage. This is dissimilar to the single-exit cascade inlet (fig. 6).

CONCLUDING REMARKS

An experimental investigation was conducted at a Mach number near 3 to ascertain the performance of several two-dimensional cascade-type inlets. The inlets were staggered at the initial shock angle. One cascade inlet discharged the flow at the subsonic diffuser exit into a common chamber, another discharged the flow into three completely separate settling chambers. The following are the results obtained from the investigation:

1. The total-pressure recovery and the mass-flow ratio of the cascade inlet with a common plenum were 0.56 and 0.99, respectively. A single element yielded a peak recovery of 0.59 and near-maximum mass flow. A single large inlet capturing about the same mass flow as the cascade yielded a peak recovery and a mass-flow performance of 0.62 and 0.99, respectively.
2. Even though there are subcritical regions of mass flow for which there is fairly stable operation (settling chamber pressure fluctuations on the order of 6 percent exist) the inlet displayed large discontinuities in total pressures at various operating conditions. These may be large enough to prevent operation of the engine subcritically.
3. The profile distortion of the cascade inlet at critical operation was 14.5 percent at the diffuser exit and 3.6 percent at a station that is further upstream than the point at which the single-passage comparison inlet yielded a distortion of 10 percent.

4. The critical and supercritical performances of a cascade inlet modified to discharge into separate plenums were approximately the same at zero angle of attack as the cascade with a common plenum.

5. The positive angle-of-attack performance of the two cascade diffusers was poor, dropping the total-pressure recovery from 56 percent at zero angle of attack to about 27 percent at 6° angle of attack. At -3° angle of attack, total-pressure recovery was approximately 44 percent.

Since the model tested was not large enough to apply boundary-layer suction conveniently, the question remains whether boundary-layer control could significantly affect the presented results.

If the suction mass flow is several percent of the captured mass flow (realistic for moderate internal contraction inlets), boundary-layer separation in the subsonic diffuser could possibly be controlled. Critical total-pressure recovery would then be near that obtained in the single-passage inlet, that is, about 0.60. If allowance is made for the removal of low-energy air, an additional count or two may be gained. Consequently, a total-pressure recovery increase of from 0.02 to 0.05 might be realized. For much the same reason, profile distortions would probably improve somewhat.

Although subcritical pressure fluctuations might be reduced to insignificant values with boundary-layer control (ref. 3), the discontinuity of pressure and mass flow that occurs just past the critical point would still exist. The discontinuity is not a viscous effect; it is controlled by diffuser exit static pressures and mass-flow relations (ref. 4). Such an inviscid effect could not be controlled by small amounts of boundary-layer removal. Since the amplitudes of the pressure fluctuations are not exceedingly large in the present investigation, suction would improve subcritical total-pressure recovery only a few counts.

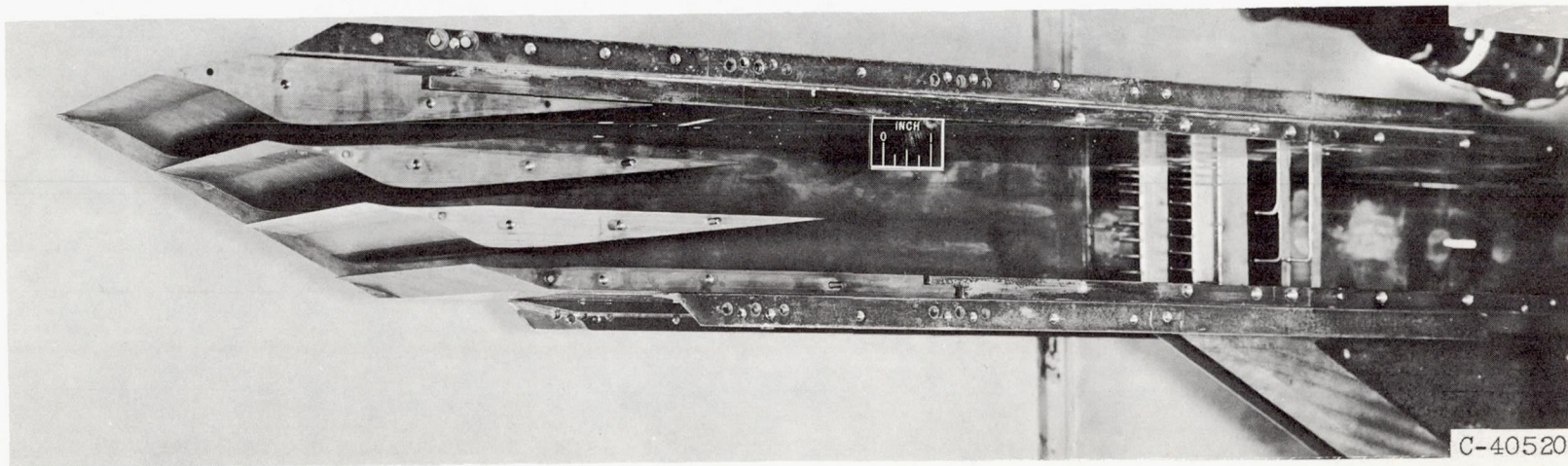
The poor positive angle-of-attack performance is another primarily inviscid effect due mainly to an increased free-stream capture tube of air and it probably could not be improved by boundary-layer bleed.

Thus, in conclusion, the effect of boundary-layer control would probably only improve recovery from 0.02 to 0.05, may decrease subcritical pressure fluctuations, and might improve the profile distortions slightly. It would have little effect upon the character of subcritical and angle-of-attack performance.

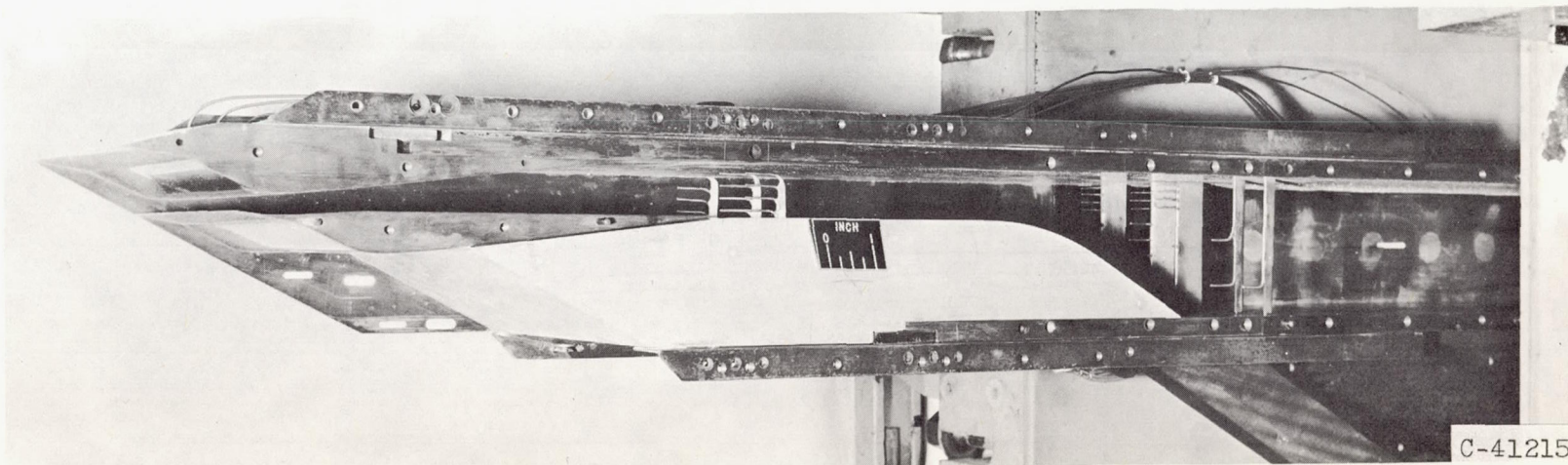
Lewis Flight Propulsion Laboratory
National Advisory Committee for Aeronautics
Cleveland, Ohio, December 9, 1957

4406
REFERENCES

1. Offenhartz, Edward: An Experimental Investigation of Two-Dimensional, Supersonic Cascade-Type Inlets at a Mach Number of 3.11. NACA RM L54E17, 1954.
2. Woollett, Richard R., and Connors, James F.: Zero-Angle-of-Attack Performance of Two-Dimensional Inlets Near Mach Number 3. NACA RM E55K01, 1956.
3. Connors, James F., and Meyer, Rudolph C.: Performance Characteristics of Axisymmetric Two-Cone and Isentropic Nose Inlets at Mach Number 1.90. NACA RM E55F29, 1955.
4. Beke, Andrew: Criteria for Initial Flow Reversal in Symmetrical Twin-Intake Air-Induction Systems Operating at Supersonic Speeds. NACA RM E55L02a, 1956.



(a) Cascade inlet.



(b) Single passage inlet.

Figure 1. - Experimental inlets; one side plate removed.

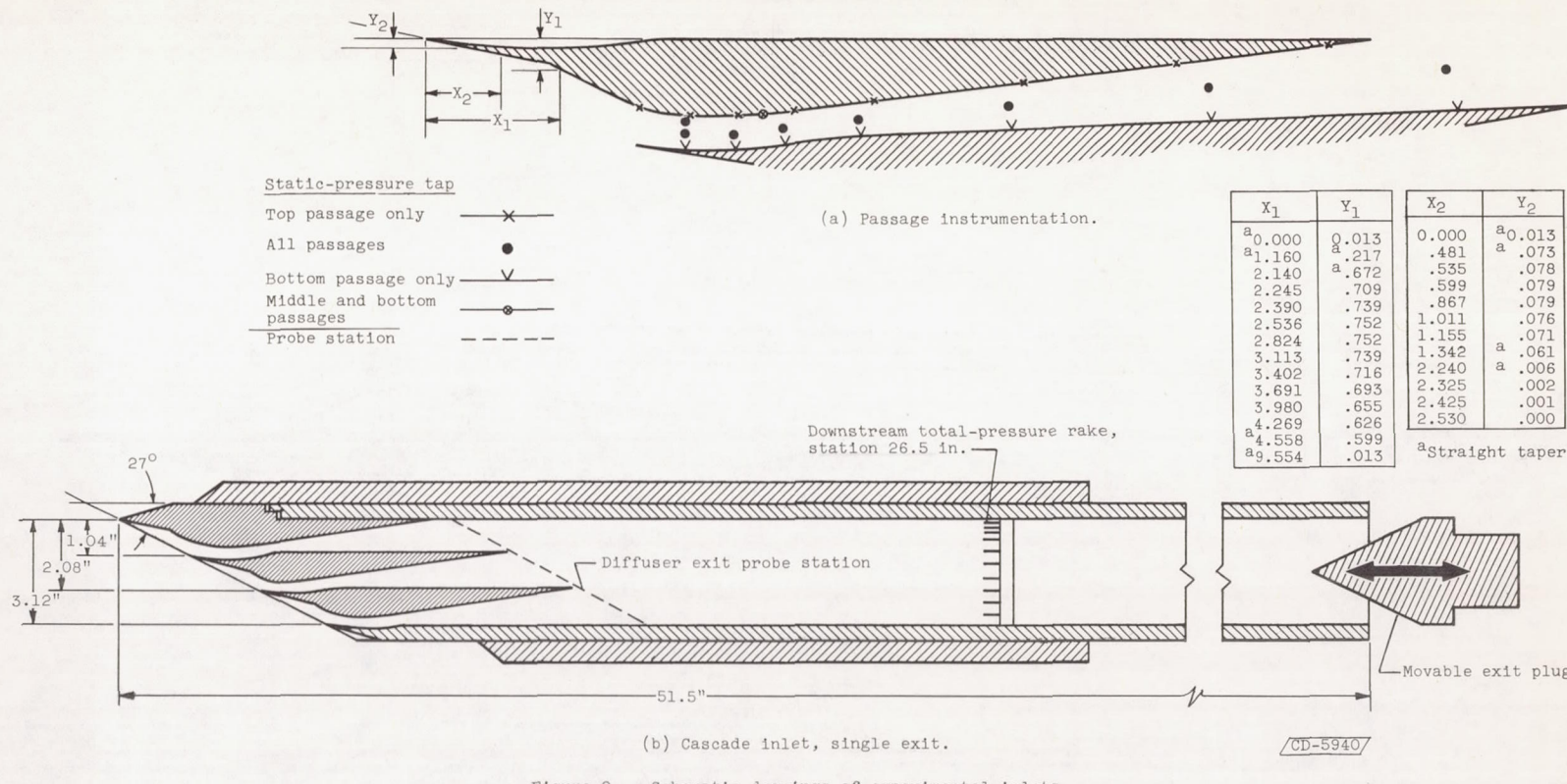
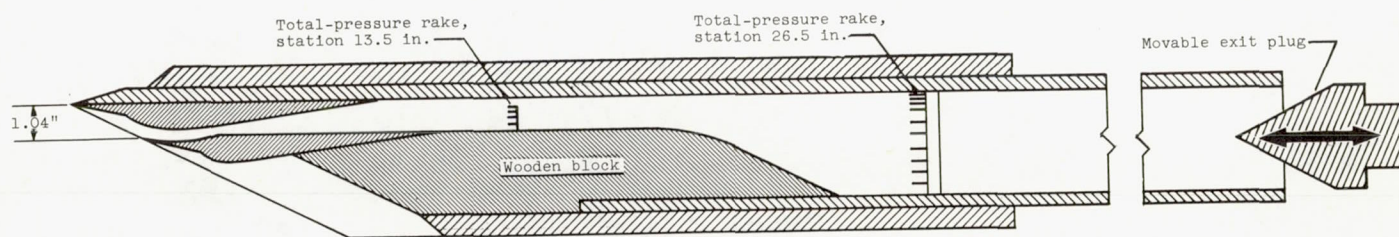
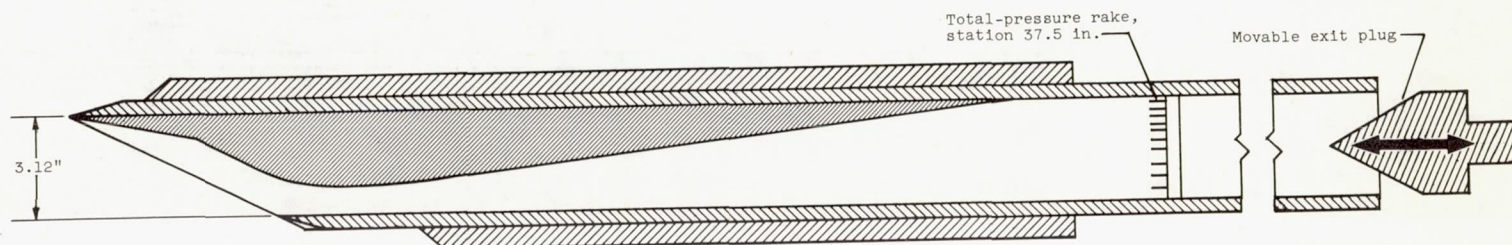


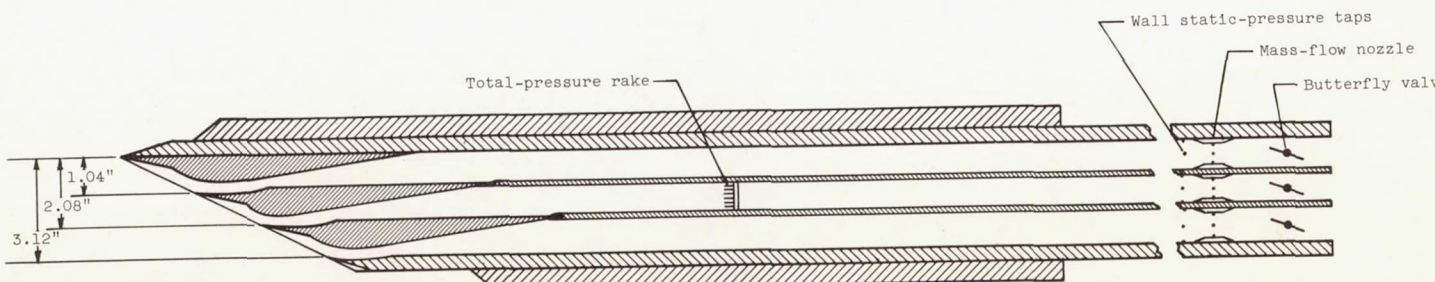
Figure 2. - Schematic drawings of experimental inlets.



(c) Single-element cascade.

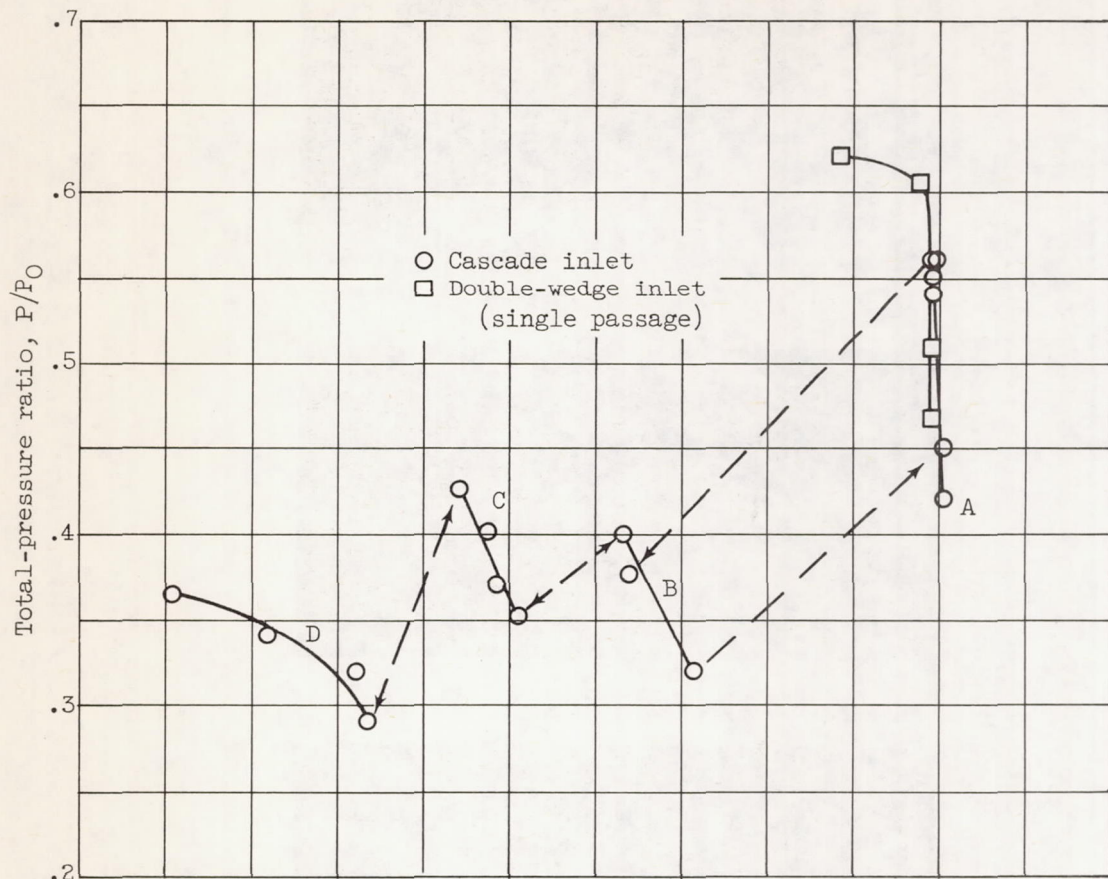


(d) Single-passage comparison inlet.

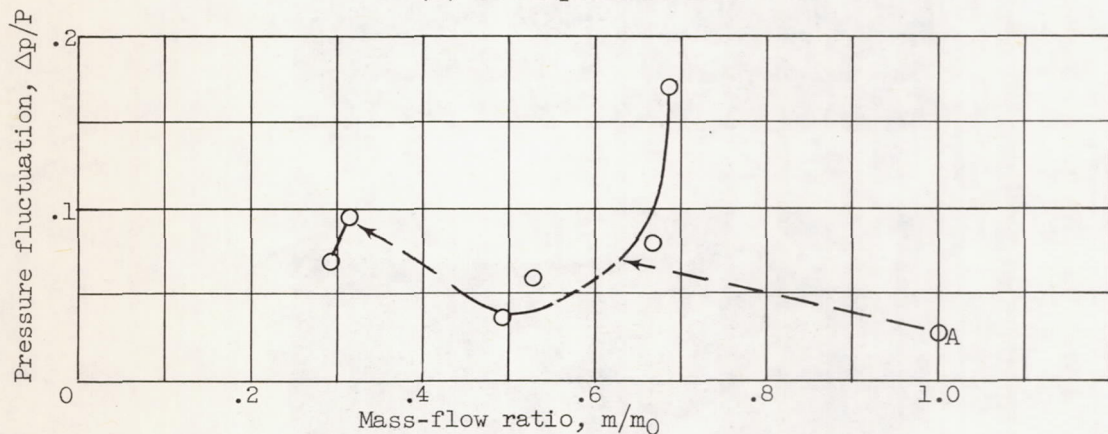


(e) Cascade inlet, triple exit.

Figure 2. - Concluded. Schematic drawings of experimental inlets.

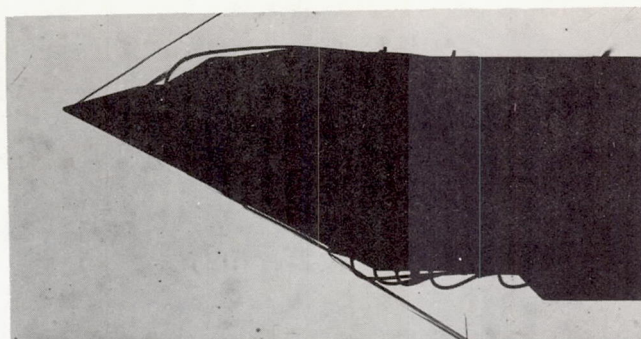


(a) Total-pressure ratio.

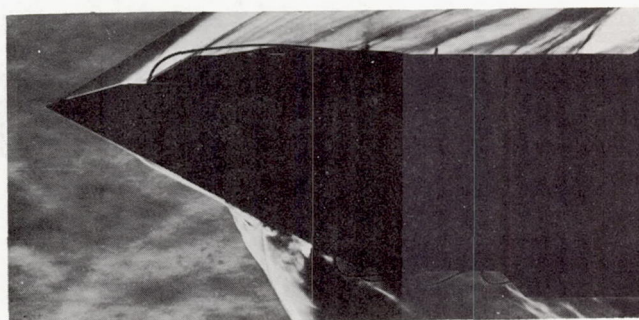


(b) Pressure fluctuations in settling chamber.

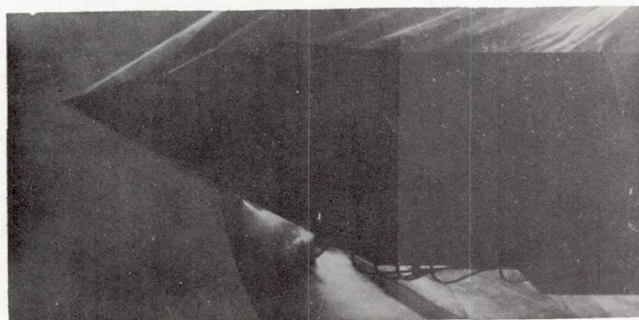
Figure 3. - Performance of cascade inlet; free stream Mach number, 3.05; zero angle of attack; ratio of entrance to throat area, 1.19.



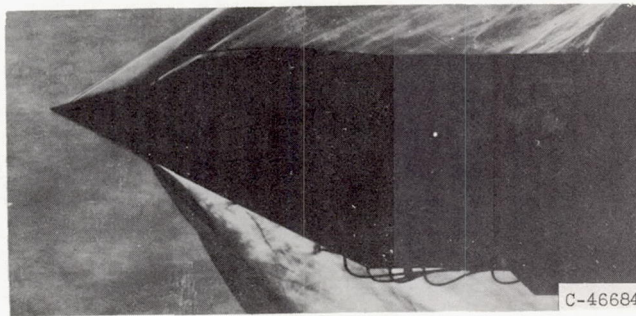
(a) Mass-flow ratio, 0.99; total-pressure ratio, 0.56;
branch A.



(b) Bottom passage subcritical; mass-flow ratio, 0.64;
total-pressure ratio, 0.375; branch B.



(c) Bottom passage subcritical; mass-flow ratio, 0.48;
total-pressure ratio, 0.37; branch C.



(d) Bottom and middle passages subcritical; mass-flow
ratio, 0.32; total-pressure ratio, 0.32; branch D.

Figure 4. - Schlieren photographs of cascade inlet; free
stream Mach number, 3.05; zero angle of attack; ratio
of entrance to throat area, 1.19.

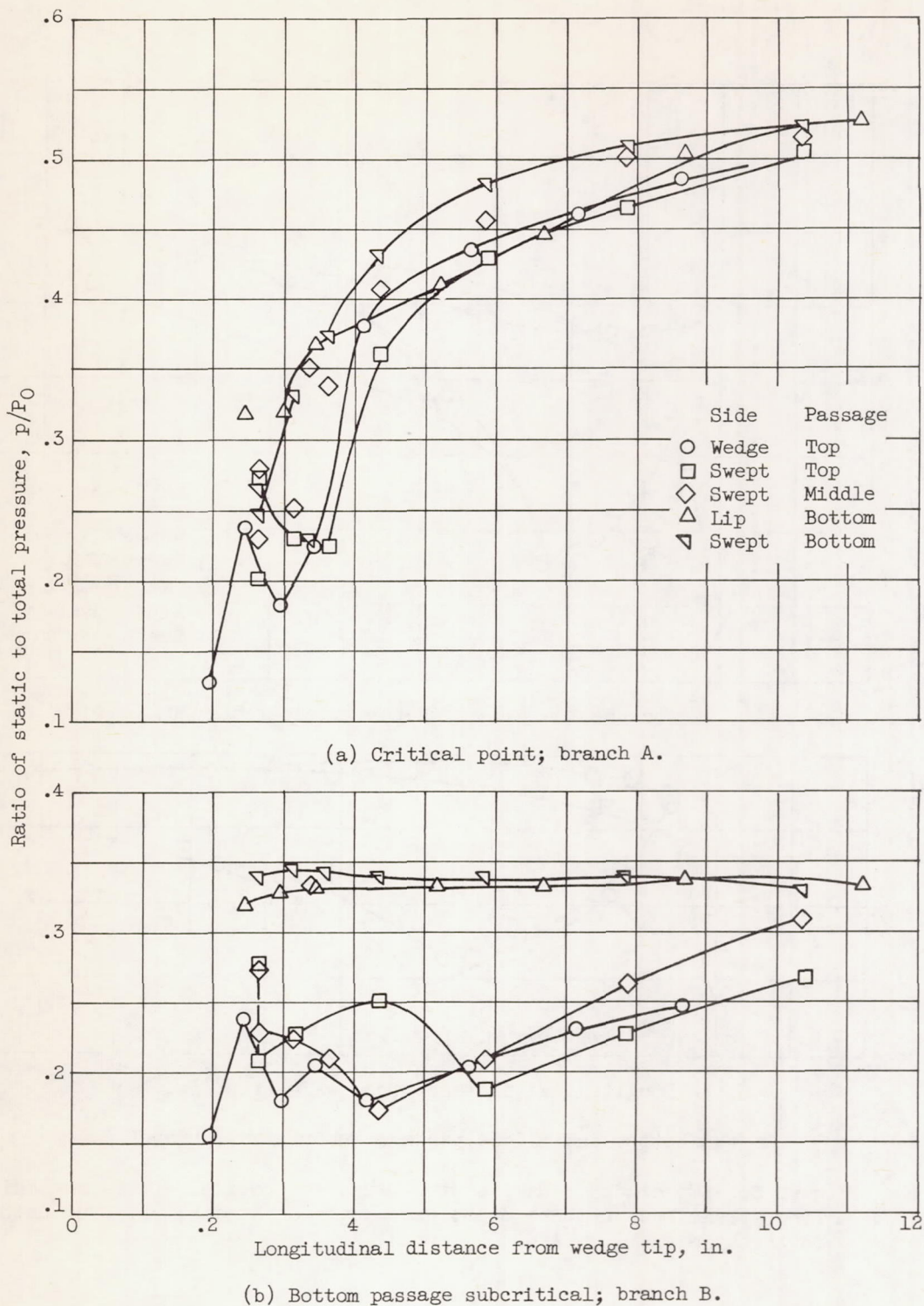
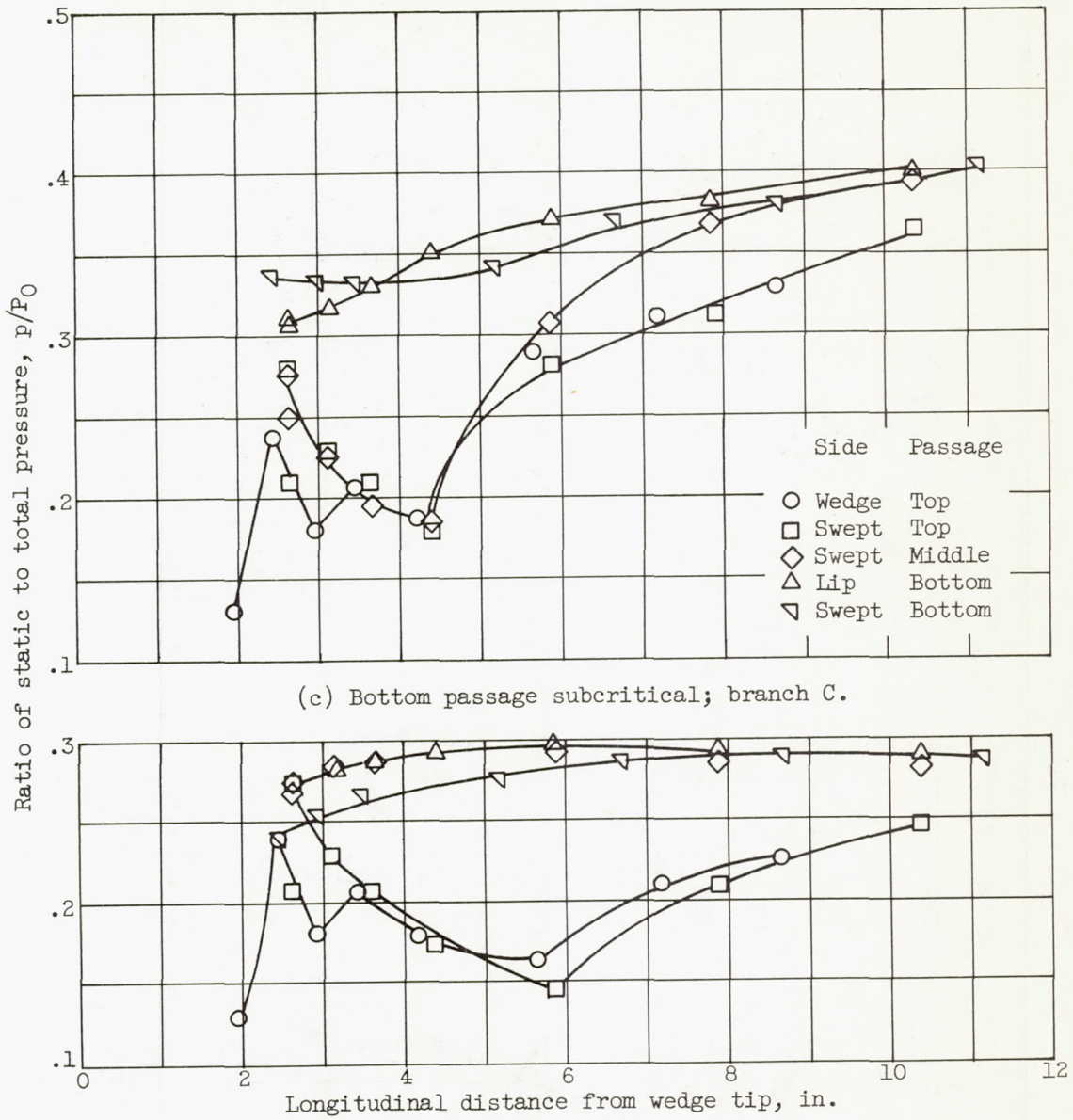


Figure 5. - Wall static-pressure profiles of cascade inlet; free stream Mach number, 3.05; zero angle of attack; ratio of entrance to throat area, 1.19.



(d) Bottom and middle passage subcritical; branch D.

Figure 5. - Concluded. Wall static-pressure profiles of cascade inlet; free stream Mach number, 3.05; zero angle of attack; ratio of entrance to throat area, 1.19.

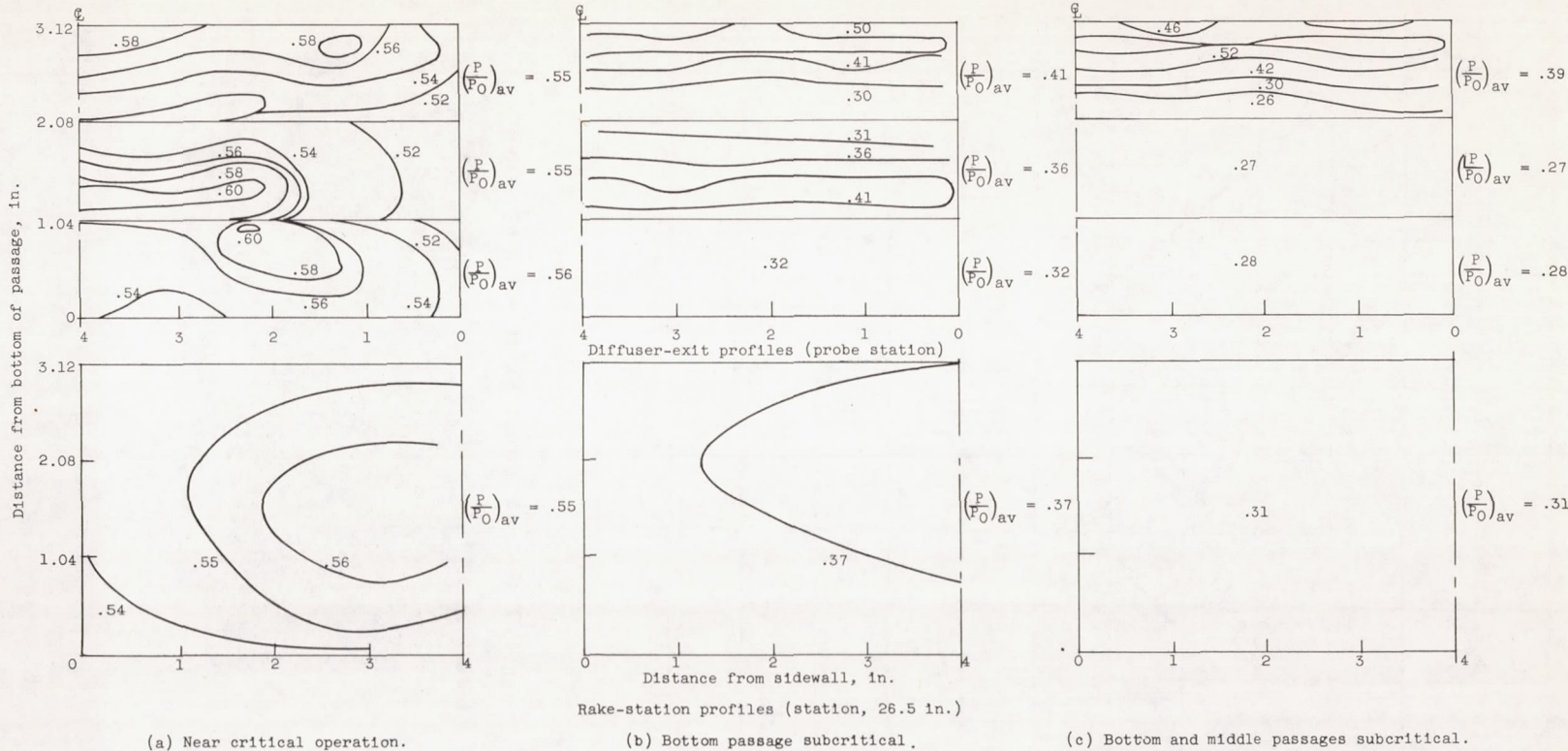
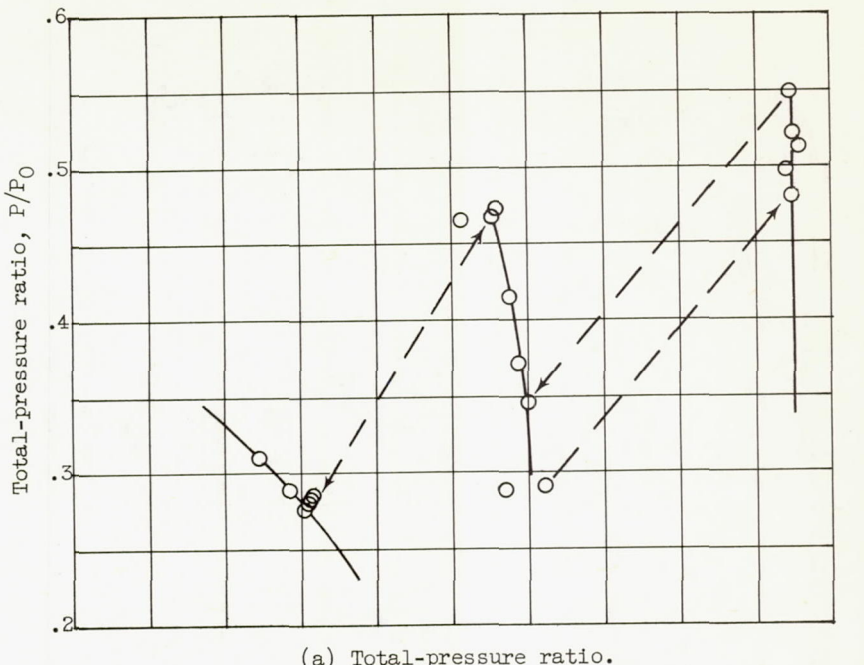
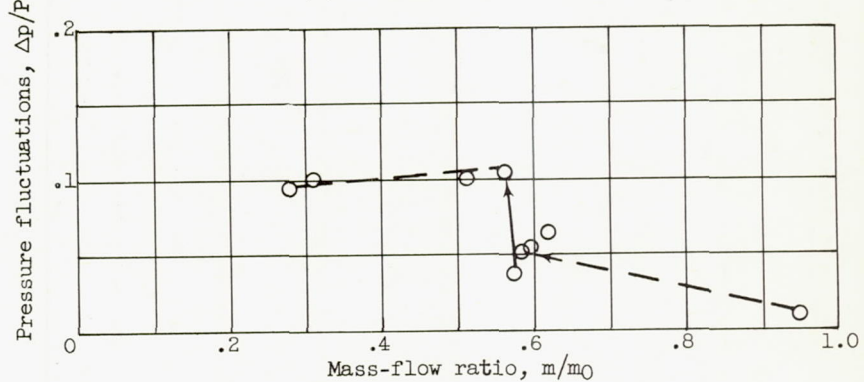


Figure 6. - Total-pressure profiles of cascade inlet profiles (looking downstream) of cascade inlet; free stream Mach number, 3.05; zero angle of attack; ratio of entrance to throat area, 1.19.



(a) Total-pressure ratio.



(b) Pressure fluctuations in settling chamber.

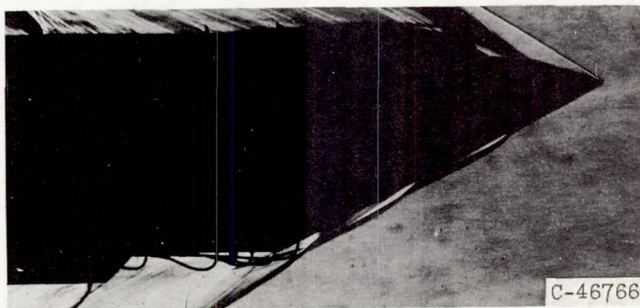
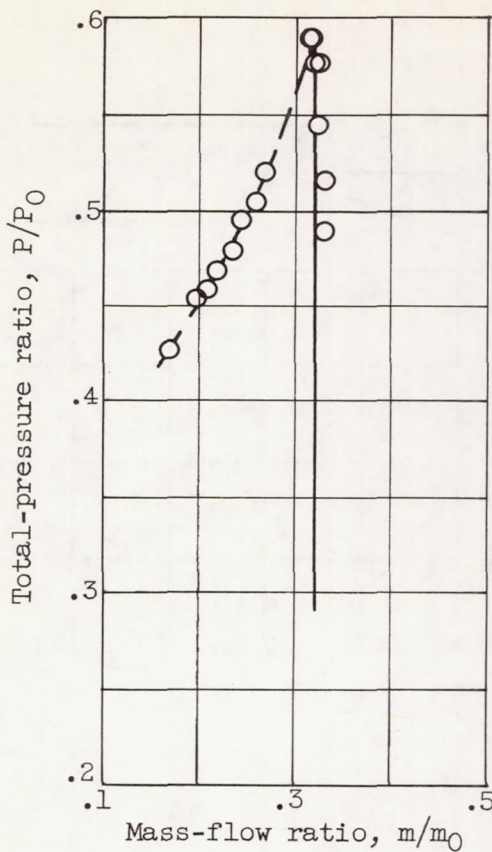
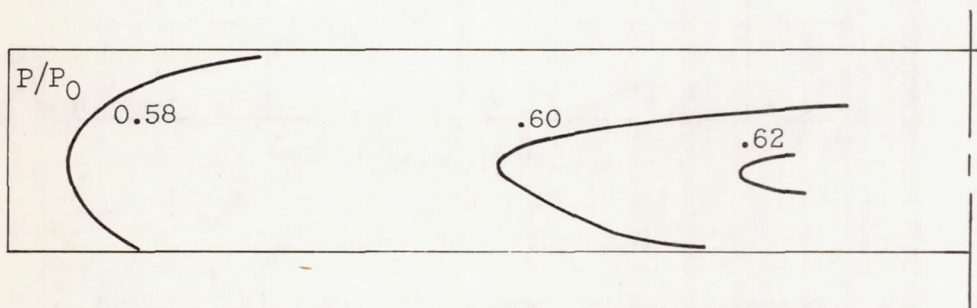
(c) Schlieren photograph; m/m_0 , 0.95; P/P_0 , 0.48.

Figure 7. - Performance of cascade inlet; free stream Mach number, 3.05; zero angle of attack; ratio of entrance to throat area, 1.09.



(a) Total-pressure recovery.



(b) Total-pressure profile.

Figure 8. - Performance of single element of cascade inlet; free stream Mach number, 3.05; zero angle of attack; ratio of entrance to throat area, 1.19.

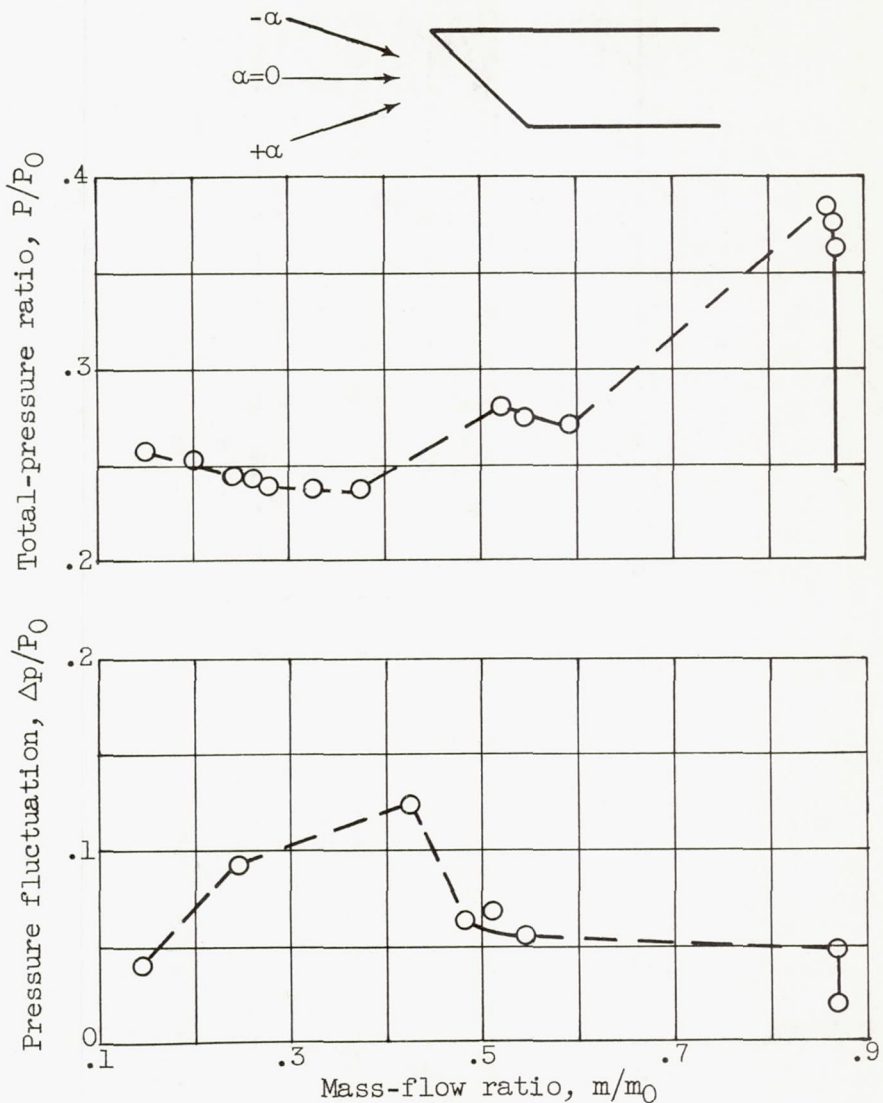
(a) Angle of attack, 3° .

Figure 9. - Performance of cascade inlet; free stream Mach number, 3.05; angle of attack, 3° ; ratio of entrance to throat area, 1.19.

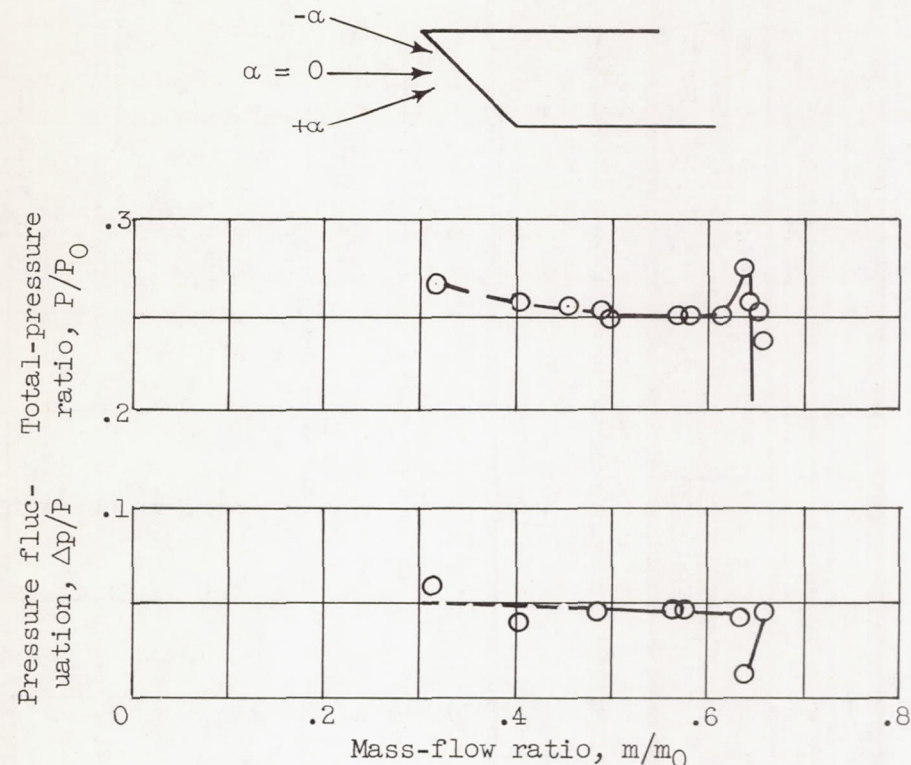
(b) Angle of attack, 6° .

Figure 9. - Continued. Performance of cascade inlet; free stream Mach number, 3.05; angle of attack, 6° ; ratio of entrance to throat area, 1.19.

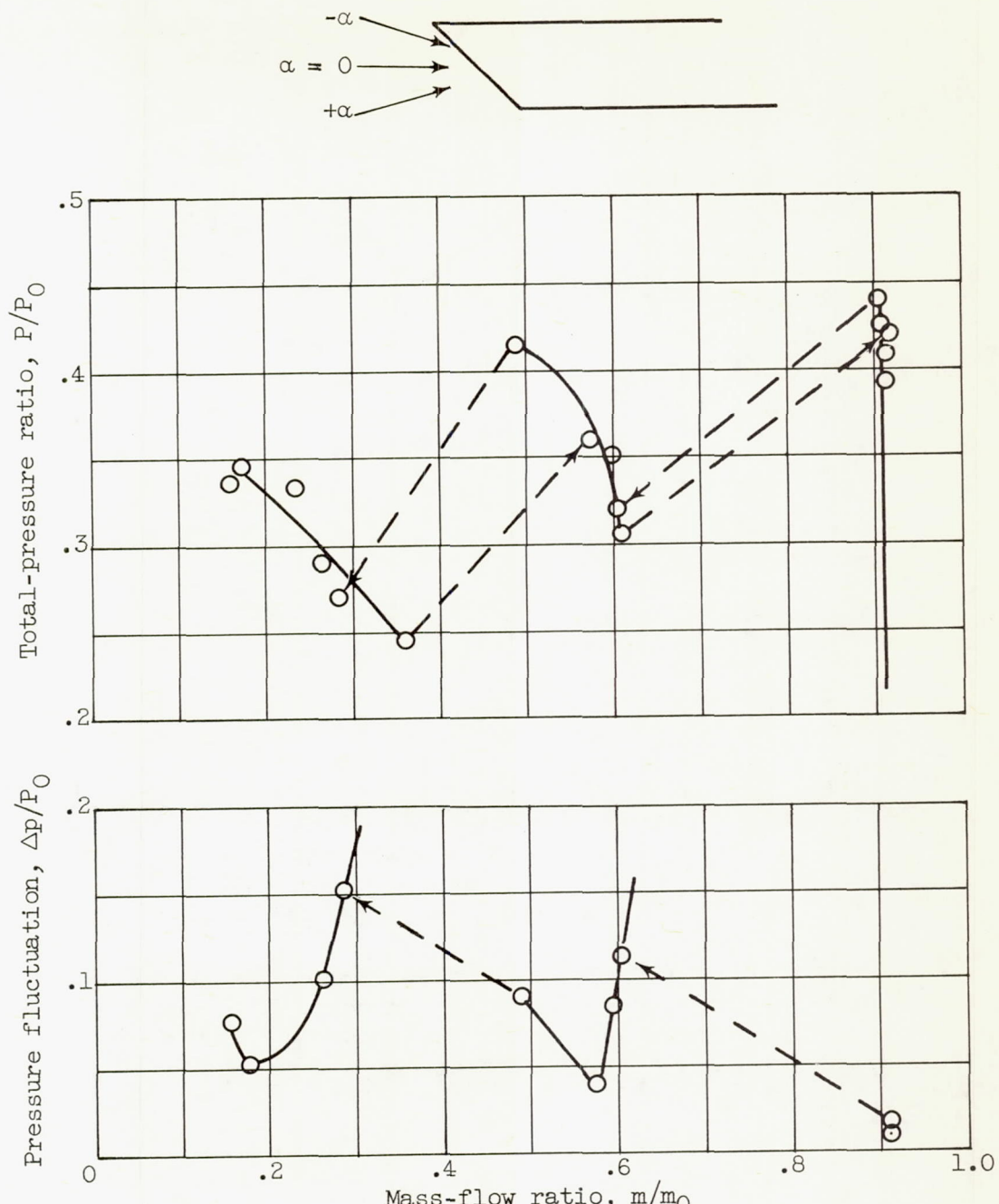
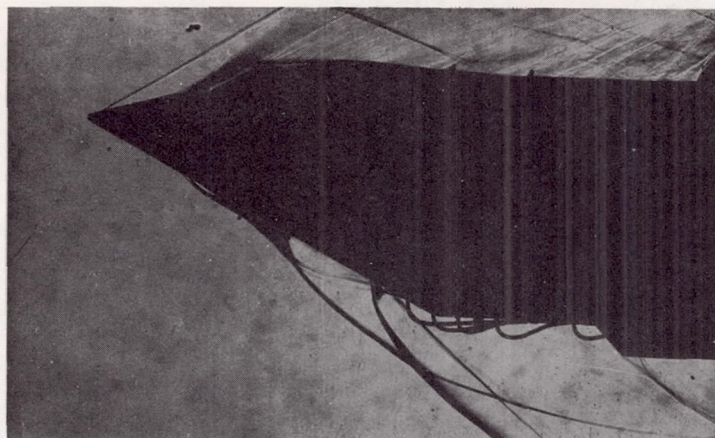
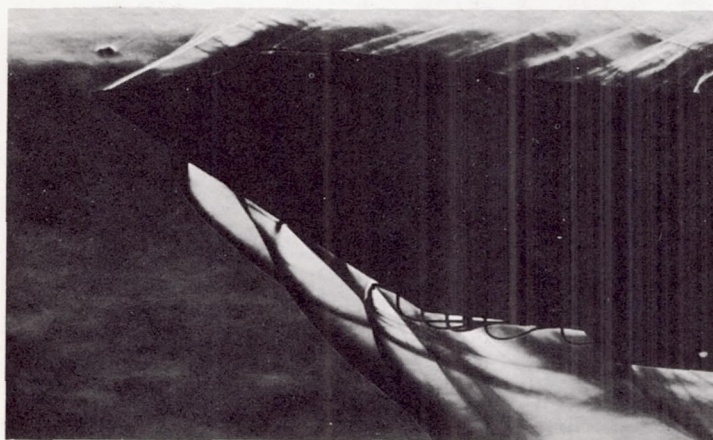
(c) Angle of attack, -3° .

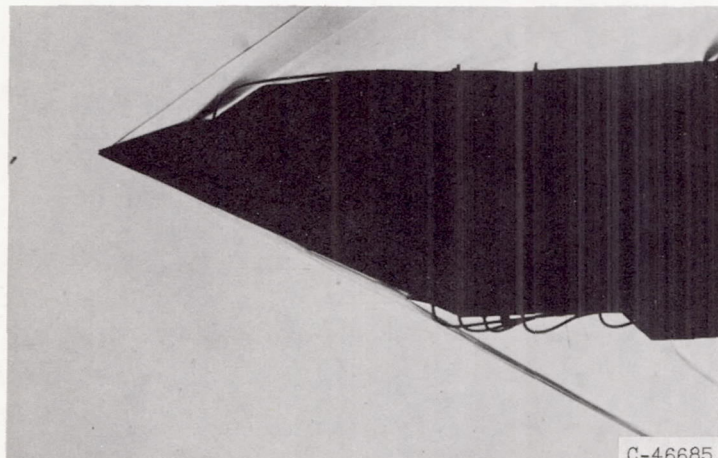
Figure 9. - Concluded. Performance of cascade inlet; free stream Mach number, 3.05; angle of attack, -3° ; ratio of entrance to throat area, 1.19.



(a) Mass-flow ratio, 0.87; total-pressure ratio, 0.36;
angle of attack, 30° .



(b) Mass-flow ratio, 0.64; total-pressure ratio, 0.26;
angle of attack, 6° .



(c) Mass-flow ratio, 0.92; total-pressure ratio, 0.39;
angle of attack, -3° .

Figure 10. - Schlieren photographs of cascade inlet; free stream Mach number, 3.05; various angles of attack.

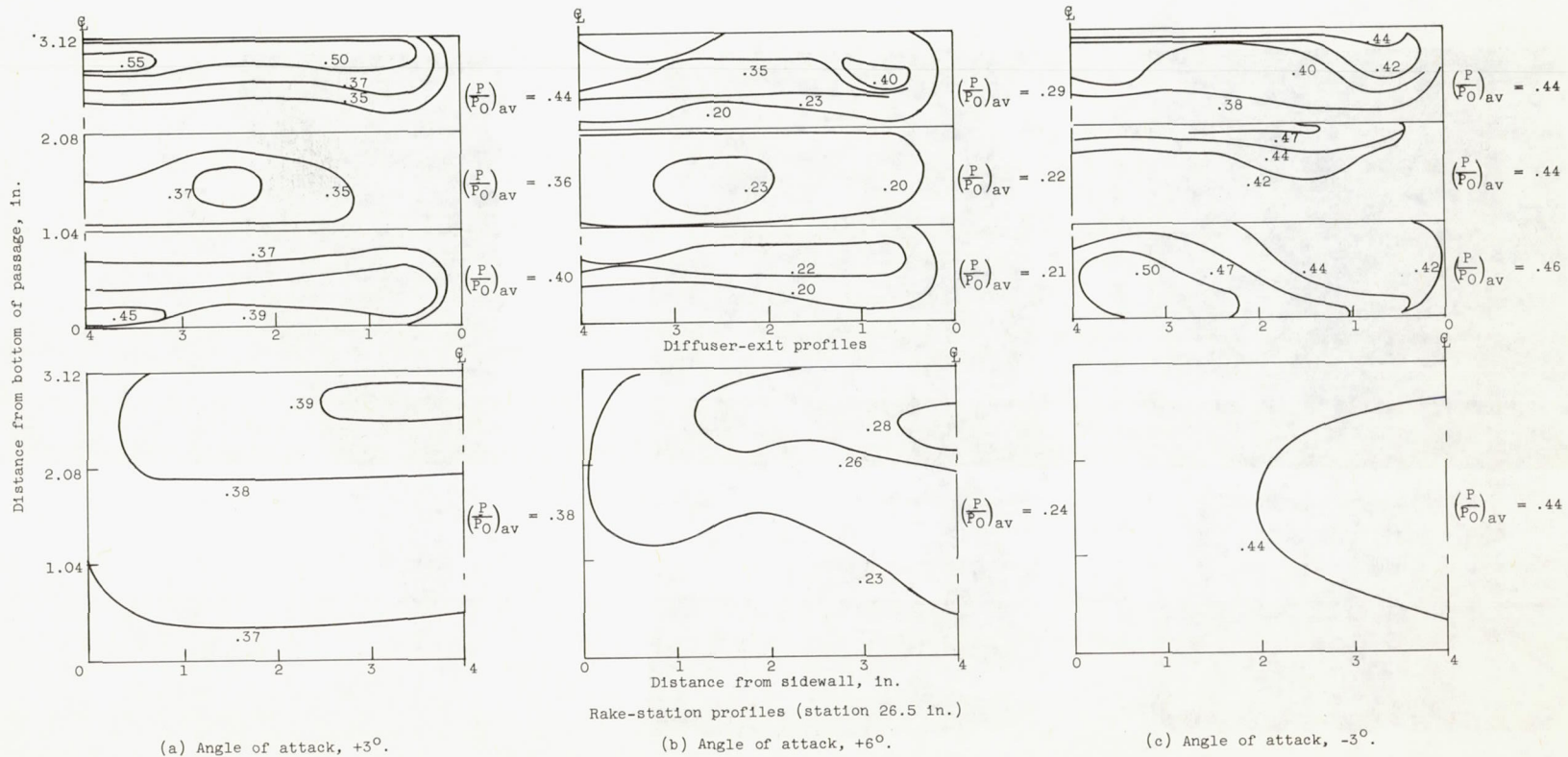


Figure 11. - Total-pressure profiles of cascade inlet profiles (looking downstream) of cascade inlet at various angles of attack; free stream Mach number, 3.05; ratio of entrance to throat area, 1.19.

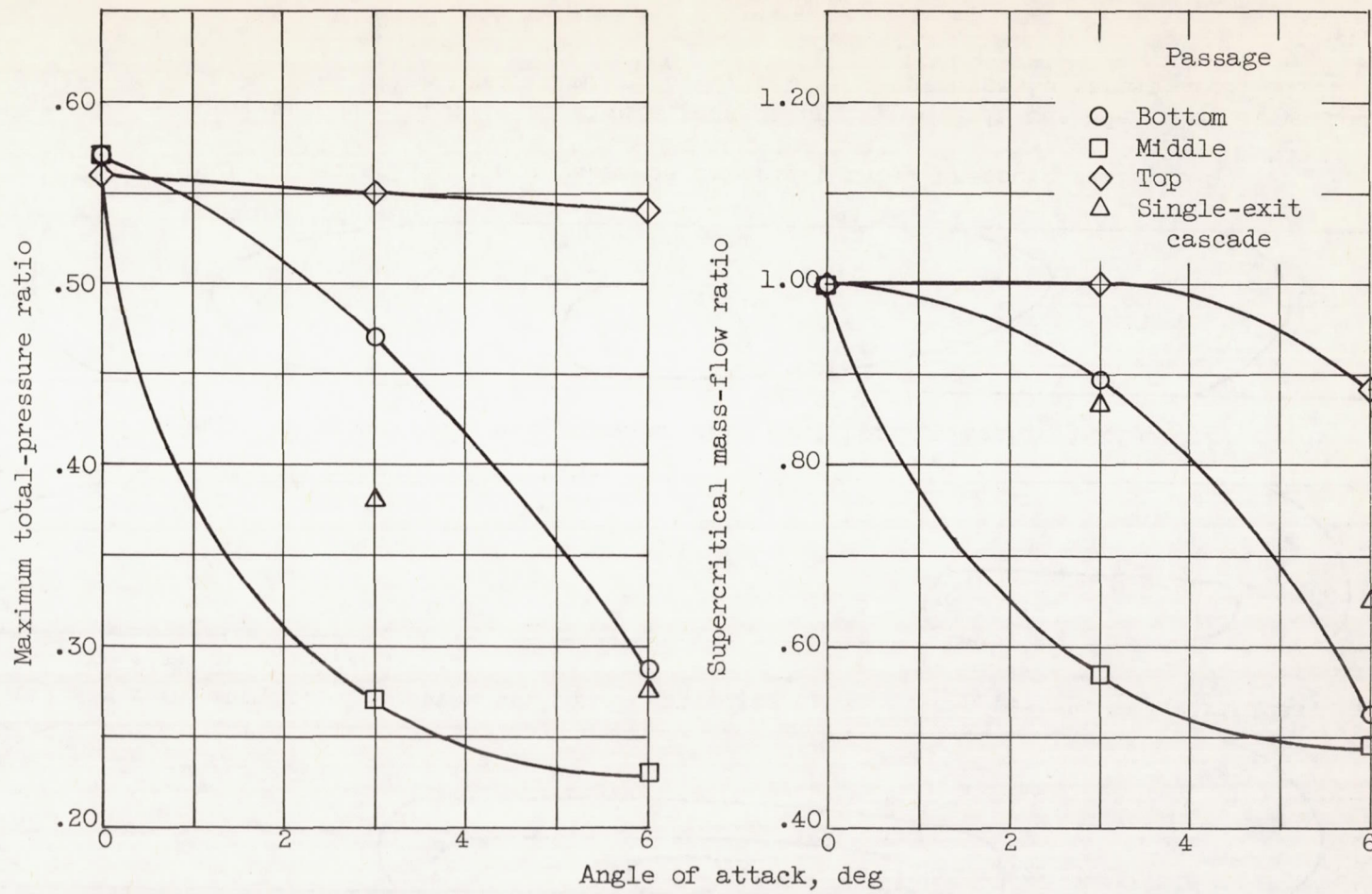
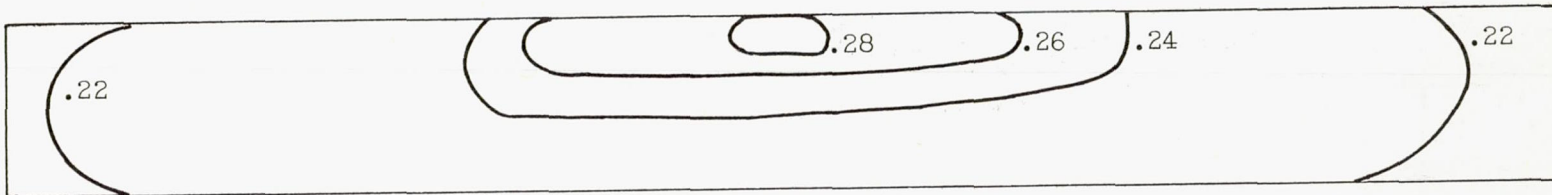
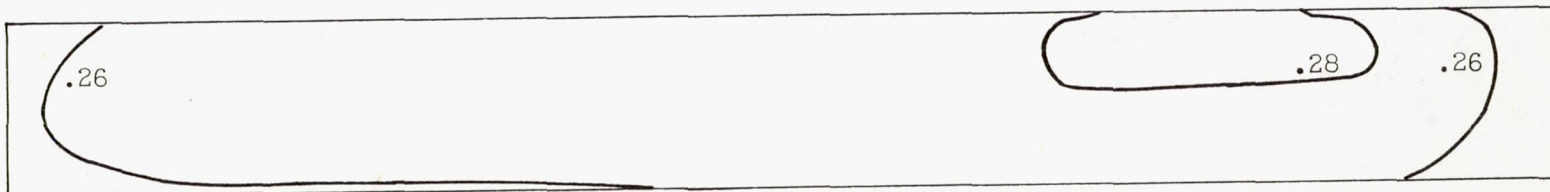


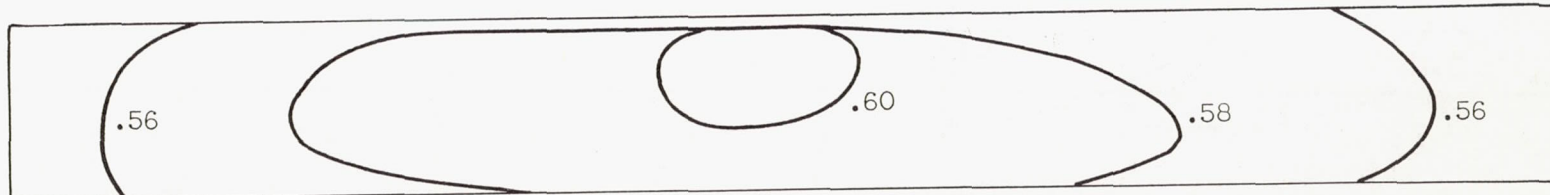
Figure 12. - Total-pressure and mass-flow variation with angle of attack for the cascade inlet with triple exit; free stream Mach number, 3.05; ratio of entrance to throat area, 1.19.



(a) Angle of attack, 6° ; bottom and middle passages critical top passage supercritical; total pressure ratio, 0.24.



(b) Angle of attack, 3° ; all passages critical; total pressure ratio, 0.27.



(c) Angle of attack, 0° ; all passages critical; total pressure ratio, 0.58.

Figure 13. - Total-pressure profile of middle passage of triple-exit cascade inlet at various angles of attack; free stream Mach number, 3.05; ratio of entrance to throat area, 1.19.

NOTES: (1) Reynolds number is based on the diameter of a circle with the same area as that of the capture area of the inlet.

(2) The symbol * denotes the occurrence of buzz.

Report and facility	Description			Test parameters				Test data				Performance		Remarks	
	Configuration	Number of oblique shocks	Type of boundary-layer control	Free-stream Mach number	Reynolds number $\times 10^{-6}$	Angle of attack, deg	Angle of yaw, deg	Drag	Inlet-flow profile	Discharge-flow profile	Flow picture	Maximum total-pressure recovery	Mass-flow ratio		
LM E57L06 Lewis 18-by 18-in. supersonic wind tunnel		2	None	3.05	0.4	-3 0 3 6	0				✓		0.56	0.1* to 1.0	The inlet displayed large discontinuities in total pressures at various operating conditions.
RM E57L06 Lewis 18-by 18-in. supersonic wind tunnel		2	None	3.05	0.4	-3 0 3 6	0				✓		0.56	0.1* to 1.0	The inlet displayed large discontinuities in total pressures at various operating conditions.
RM E57L06 Lewis 18-by 18-in. supersonic wind tunnel		2	None	3.05	0.4	-3 0 3 6	0				✓		0.56	0.1* to 1.0	The inlet displayed large discontinuities in total pressures at various operating conditions.
RM E57L06 Lewis 18-by 18-in. supersonic wind tunnel		2	None	3.05	0.4	-3 0 3 6	0				✓		0.56	0.1* to 1.0	The inlet displayed large discontinuities in total pressures at various operating conditions.

Bibliography

These strips are provided for the convenience of the reader and can be removed from this report to compile a bibliography of NACA inlet reports. This page is being added only to inlet reports and is on a trial basis.